

Journal of Biomedical Optics

BiomedicalOptics.SPIEDigitalLibrary.org

Dynamic phase differences based on quantitative phase imaging for the objective evaluation of cell behavior

Aneta Krizova
Jana Collakova
Zbynek Dostal
Lukas Kvasnica
Hana Uhlirova
Tomas Zikmund
Pavel Vesely
Radim Chmelik

Dynamic phase differences based on quantitative phase imaging for the objective evaluation of cell behavior

Aneta Krizova,^{a,b,*} Jana Collakova,^{a,b} Zbynek Dostal,^{a,b} Lukas Kvasnica,^a Hana Uhlirova,^c Tomas Zikmund,^{a,b} Pavel Vesely,^{b,†} and Radim Chmelik^{a,b,†}

^aBrno University of Technology, Institute of Physical Engineering, Faculty of Mechanical Engineering, Technicka 2896/2, Brno 61600, Czech Republic

^bBrno University of Technology, CEITEC—Central European Institute of Technology, Technicka 3058/10, Brno 61600, Czech Republic

^cUniversity of California San Diego, 9500 Gilman Drive, La Jolla, California 92093, United States

Abstract. Quantitative phase imaging (QPI) brought innovation to noninvasive observation of live cell dynamics seen as cell behavior. Unlike the Zernike phase contrast or differential interference contrast, QPI provides quantitative information about cell dry mass distribution. We used such data for objective evaluation of live cell behavioral dynamics by the advanced method of dynamic phase differences (DPDs). The DPDs method is considered a rational instrument offered by QPI. By subtracting the antecedent from the subsequent image in a time-lapse series, only the changes in mass distribution in the cell are detected. The result is either visualized as a two-dimensional color-coded projection of these two states of the cell or as a time dependence of changes quantified in picograms. Then in a series of time-lapse recordings, the chain of cell mass distribution changes that would otherwise escape attention is revealed. Consequently, new salient features of live cell behavior should emerge. Construction of the DPDs method and results exhibiting the approach are presented. Advantage of the DPDs application is demonstrated on cells exposed to an osmotic challenge. For time-lapse acquisition of quantitative phase images, the recently developed coherence-controlled holographic microscope was employed. © 2015 Society of Photo-Optical Instrumentation Engineers (SPIE) [DOI: 10.1117/1.JBO.20.11.111214]

Keywords: holographic microscopy; quantitative phase imaging; live cell behavior evaluation; dynamic phase differences; osmotic challenge.

Paper 150151SSR received Mar. 12, 2015; accepted for publication Aug. 5, 2015; published online Sep. 3, 2015.

1 Introduction

For observation and evaluation of live cell behavior, methods such as Zernike phase contrast or differential interference contrast (DIC) that improve the contrast of unstained cells are widely used. The improvement of contrast has only a qualitative meaning and pixel values in these images do not have a clear relation to the physical properties of observed objects. This drawback is currently eliminated by techniques of quantitative phase imaging (QPI). With these techniques, the phase shift caused by the inspected sample is precisely measured. The phase shift corresponds to an optical path difference which is given by the refractive index and the cell height.¹ Different laborious methods^{2–5} have been developed for decoupling these parameters that are not easily distinguishable. Fortunately, the phase shift in radians can be straightforwardly recalculated to the cell dry mass in picograms without the need for decoupling these parameters. Cell dry mass represents the nonaqueous material which mainly depends on protein concentration in the cell structures and was defined as the weight of the cell when water had evaporated.⁶ Interpretation of phase shifts in terms of cell dry mass is widely used in cell biology studies by QPI.^{7–10} Moreover, a meaningful application of the difference

method detecting changes between two digital images for measurement of live cell dynamics *in vitro* was already mentioned as an option for computerized image processing,¹¹ and used in a specific study limited to the activities of cell protrusions and retractions.¹² With the dynamic phase differences (DPDs) method based on QPI, the resulting information about changes in cellular dry mass and their topographical distribution over the whole projection of the cell represents an advance in the objective characterization of cell behavior *in vitro*. Cell motility that also covers the internal translocation of cell dry mass can also be better described by the impressions and measurements gained only from changes of the cell dry mass that are clearly defined by color coding. Such a visualization is crucial because it reveals features that are imperceptible by simple comparison of subsequent quantitative phase images.

In our first attempt,¹³ the reaction of cells to nutritional stress was evaluated by the basic DPD method. The basic DPD method compared chosen subsequent frames of an ongoing cellular dynamic process by subtracting the antecedent image from the subsequent. The difference found quantitatively showed the overall change in terms of cell dry mass in picograms. Then, if the difference is projected into color-coded visualization, the individual cell states depicting their fates over a chosen time interval were presented.

*Address all correspondence to: Aneta Krizova, E-mail: aneta.krizova@ceitec.vutbr.cz

†These authors share senior authorship.

Now, a coherence-controlled holographic microscope (CCHM)¹⁴ with more developed hardware^{15,16} and image processing software¹⁷ provides a much more robust tool for the cell dry mass measurement. Hence, our current advanced DPDs method can be based on the upgraded quality of the QPI. We can, thus obtain reliable data for the calculation of the difference between deliberately chosen cell states. Consequently, the advanced DPDs method presents more reliable numerical data in picograms about a stream of cell dry mass variation amenable to further statistical processing and/or fast appreciation by percent normalization. The color-coded data distribution produces detailed topographical information about the dynamics of cell behavior. Such novel knowledge promises criteria for the elaboration of an innovative objective classification of cell behavior *in vitro*.

2 Materials and Methods

2.1 Cell Culture

Spontaneously transformed rat embryonic fibroblasts LW13K2¹⁸ were grown attached to a solid TC surface. Standard medium M1H [Eagle's MEM based on Hanks balanced salt solution (BSS) enriched with nonessential amino acids and 1-mM sodium pyruvate, with 1-g NaHCO₃/L and 10% calf serum] and transfers to new culture vessels by trypsinization were used. For microscopic measurements, cells were seeded into flow chambers μ -Slide I Luer Family cat. num. 80196 (Ibidi, Martinsried, Germany) in standard medium. Before observations, the standard medium was exchanged for F10 medium (Eagle's MEM w/o phenol red based on Hanks BSS enriched with nonessential amino acids and 1-mM sodium pyruvate, with 0.3-g NaHCO₃/L, 20-mM nonvolatile buffer TES Sigma T5691, and 10% calf serum). For a hypo-osmotic challenge, standard tissue culture water was used to dilute the F10 medium.

2.2 Quantitative Phase Imaging

Briefly, QPI was performed by CCHM. CCHM is designed as an off-axis setup and only one hologram is needed for image reconstruction.^{14,15} For illumination, a halogen lamp source and interference filter with a central wavelength 650 nm and FWHM 10 nm were used. Objectives Nikon Plan 10 \times /0.3 and a CCD camera (XIMEA MR4021MC-VELETA) were used to capture holograms. The holograms were numerically reconstructed and processed using house-built software. The cells were segmented from the background, followed by the measurements of the cell dry mass and DPDs calculation.

The cells were observed in flow chambers μ -Slide I Luer Family cat. num. 80196 (Ibidi, Martinsried, Germany) and a house-built pump was used for perfusion of media. The velocity of the perfused media was 0.4 ml/min.

2.3 Recalculation of Phase Shifts to Cell Dry Mass

As is known, a phase shift corresponds to the optical path difference that is given by the refractive index and the cell height. Live cells are composed primarily of light atoms that interact with the light in a similar manner. Owing to this, the increase in refractive index corresponds to the increase of cell dry mass, where cell dry mass is defined as the nonaqueous contents of the cell. The refractive index is directly proportional to the cell dry mass and the constant α of this proportion is called the specific refraction

increment.¹⁹ The total cell dry mass of one cell can then be calculated as an integral over the cell area⁷

$$m = \iint \frac{\text{OPD}}{100\alpha} dA,$$

where m is the total cell dry mass in pg, OPD is the optical path difference measured in μm , α is the specific refraction increment in $\mu\text{m}^3/\text{pg}$, and A is the area of the cell in μm^2 .

3 Results and Discussion

3.1 Dynamic Phase Differences

In this section, we describe newly introduced necessary data preprocessing, the used definition of the noise limitation, and the advanced DPDs calculations. The advances embrace implementation of the cell segmentation and clear visualization of the cell boundaries as well as the extension of DPDs color coding in order to distinguish newly occupied and abandoned areas by the cells.

3.1.1 Data Preprocessing

The complex record of a light wave acquired by a camera is called a hologram. From a hologram, the raw phase and amplitude are calculated using Fast Fourier transformation.²⁰ On the raw phase, common unwrapping methods are applied^{21,22} and the resulting image is called the unwrapped phase image. This image contains information about the observed object and also, unfortunately, phase deformations caused by inaccuracies of the optical system or optical elements' aberrations. The deformations are subtracted using our own method described in Ref. 17. The result after these corrections is called the compensated phase and contains only phase deformation caused by the observed object, while the background of the image has a mean value equal to zero.

Cells observed by QPI usually have rather high values of phase shift in their nuclei and nucleoli. Therefore, the highest values in the image are detected and cells are identified. Cells limited by the background threshold value and then by a minimal contiguous area can be segmented from the image. From the background, spatial and temporal noise can be calculated as described in Sec. 3.1.2. Afterward, all pixels in the background are set to zero. The image with segmented cells and zero background are the input data into the advanced DPDs calculation.

3.1.2 Definition of noise limitation

Each measurement is limited by noise. We can distinguish the temporal noise, which is fluctuations in each pixel during the time series of the observation, and the spatial noise, which is fluctuations among the pixels in one image. For DPDs evaluation, the temporal noise is significant and determines the least change of cell dry mass that can be detected. This limiting value can be different for each measurement (depends mainly on adjustment of the microscope) and, therefore, it is necessary to determine the value for each series of measurements, i.e., an experiment.

In the image sequence intended for evaluation by the DPDs method, a region of only background is chosen (a region of the cell's size and near the cell is recommended) and statistical properties of the temporal noise (average value and variance) are determined in each pixel of the region according to equations

$$\bar{\hat{x}} = \frac{1}{N} \sum_i \hat{x}_i,$$

$$\sigma_N^2 = \frac{1}{N^2} \sum_{i=1}^N (\hat{x}_i - \bar{\hat{x}})^2,$$

where σ_N^2 is the variance, N is the number of images in the sequence, \hat{x}_i is the value of the pixel in image i , and $\bar{\hat{x}}$ is the average value of this pixel in the image sequence. By calculation over the chosen region, we can get an array of variances σ_N^2 or standard deviations σ_N . The minimal measurable change of the cell dry mass is assumed to be equal to the maximal standard deviation σ_{\max} from the chosen region.

If the acquisition interval is too short, the change between two images in most cases is less than the temporal noise. Changes higher than the temporal noise occur only in isolated pixels and do not provide meaningful biological information.

3.1.3 Advanced calculations of dynamic phase differences

Assuming a time sequence of N images (compensated phase with segmented cells), then DPDs are given by the equation (array calculus)

$$\text{DPD}_{i+k} = \varphi_{i+k} - \varphi_i,$$

where φ_i is the phase image i , k is the difference step, and we consider only DPD_{i+k} bigger than σ_{\max} . DPD_{i+k} is calculable with an arbitrary step k until the step k is lower than the number N of images in the sequence.

In topographical representation, negative values of DPDs are in green color and indicate the decrease of cell dry mass. Positive values of DPDs are illustrated in red color and denote the increase of cell dry mass. Color intensity corresponds to the magnitude of the change. Differences smaller than σ_{\max} are in black while the background is in white.

This is the basic principle which is also maintained in the current extension version of DPDs.

In order to recognize abandoned and newly occupied areas, the DPDs are extended by adding another color into the current color code. In math, it means that in the couple of images, φ_i , φ_{i+k} , such areas where just one value from the pair is zero are searched. Then the corresponding nonzero value is assigned blue color. In RGB imaging, this creates a magenta color (red and blue) for newly occupied areas and a cyan color (green and blue) for abandoned areas.

An example of a biological situation where we can use the DPDs method with advantage is division of the cell. In Fig. 1,

transition between the anaphase (a) and cytokinesis (b) in QPI is depicted. In the anaphase, the formed daughter chromosomes are pulled to the opposite ends of the cell and the cell is elongated. After that, in cytokinesis, the cell is elongated even more and a cleavage furrow is clearly visible. In Fig. 1(c), this transition is visualized using extended DPDs. Newly occupied areas in the opposite ends of the dividing cell because of the elongation are in magenta color, and the decrease of mass in the area of the cleavage furrow is in cyan. For clear demonstration of the DPDs, the change in the cell dry mass distribution is also identifiable from QPI and the color code of DPDs is, therefore, more intuitive. In the experiments mentioned in Sec. 3.2, the chosen time interval between quantitative phase images is shorter and the importance of DPDs is more obvious.

3.1.4 Enumeration of mass changes in picograms

The numerical evaluation of dry mass transfers provides data that can be plotted on time-based graphs offering another characterization of cell behavior. Data can be calculated in picograms or in normalized percentage change. Both versions give similar representation. Percentage change represents the dynamics of the observed processes in general and is more easily comparable for different measurements, whereas from the graph of dry mass transfers, the dynamics of the observed processes can be seen more specifically. Figure 2 depicts both representations of mass changes in time-based graphs. In the graph with DPDs, massive translocation of the cell mass during the cell shrinkage is represented by the cyan peak (time 5 to 20 min), significant attenuation in cell activity during the mitosis is apparent from the low values of all differences (time 20 to 40 min), and cell elongation is clear from the magenta peak (time 40 to 50 min). From the graph of the percentage change, any type of the cell dynamics is readable.

We assume that the course of mitosis or other processes registered as changes of cell dry mass density over the projected area can possibly serve the automation of experiment controls.

3.1.5 Dynamic phase differences usage

Currently, three modes of DPDs application to a series of images are the incremental DPDs, the sliding DPDs, and spanning DPDs.

Incremental DPDs show the emergence and increment of the change in a series of steadily increasing intervals k between compared images. The shortest time interval that reveals a recognizable change above the noise in DPDs then serves as a comparative measure of the swiftness and quantitation of the observed events.

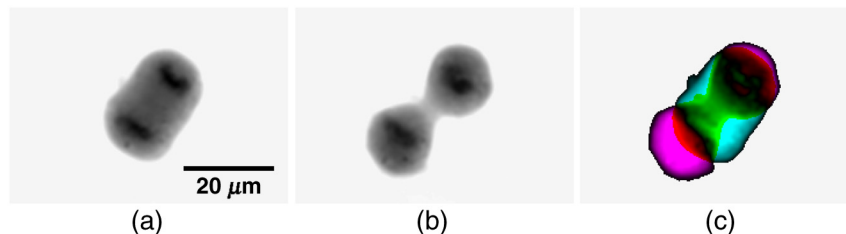


Fig. 1 Extended dynamic phase difference (DPD) of cell division with 240-s step; objectives $20\times/0.40$. QPI images of cell in (a) anaphase and (b) cytokinesis; (c) extended spanning DPDs representation of overall cell transition from (a) to (b) that catches even the slight rotation of the dividing cell around the center of the activity.

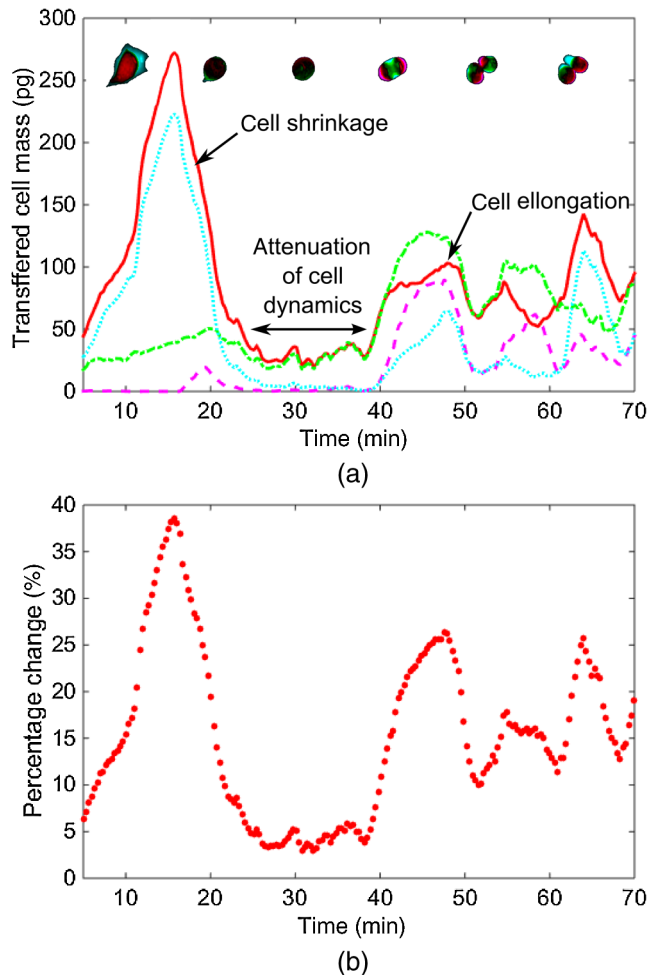


Fig. 2 LW13K2 cell cycle. (a) Representation of cell division process by a graph of values from extended DPDs. The extended spanning DPDs over 5 min are at the top. Lines depict the total amount of the change in cell dry mass at the given time points (red—amount of increased mass in cell, green—amount of decreased mass in cell, magenta—amount of mass in newly occupied area, cyan—amount of mass in abandoned area). (b) Representation of cell division process by graph of percentage changes (translocated mass over the total mass in the image) that depicts the cell dynamics regardless of the type of the dynamics. The course of mitosis registered as changes of cell dry mass density over the projected area can possibly serve the automation of experiment control.

We tested fast acquisition on our microscope with objective $10\times/0.3$. We found out that the minimal reasonable interval for acquisition is 1 s in our case of rat sarcoma cells K2 in standard culture conditions. The value of the maximal standard deviation σ_{\max} was 0.04 rad ($0.0230 \text{ pg}/\mu\text{m}^2$) and the illustration of the DPDs images is in Fig. 3, where the background is in white color, changes smaller than the noise are in yellow color, and higher changes are in red or green color. This approach enables measurement and comparison of the rate of motion between various cells in their dependence on environmental conditions.

Sliding DPDs show the regularity and frequency of the observed process in a series of chosen fixed intervals k between compared images and consequently detect the occurrence of changes that otherwise would remain unnoticed.

Spanning DPDs provide the resulting information in the proportionally graded color-coded two-dimensional (2-D) map of the detected changes and/or the calculation of transfer of the cell dry mass inside or outside the initial cell boundary over a distance. Thus, the translocation and migration of the cell is documented in a printable scheme that embraces the dynamic process. The train of color-coded changes is deemed to inspire an identification/recognition of patterns of cellular motility characteristic of so far unrecognized modes of cell behavior.

In Fig. 4, negative values of DPDs are represented in green color and indicate the decrease of cell dry mass in this area. Positive values of DPDs are illustrated in red color and denote the increase of cell dry mass in this area. Color intensity corresponds to the magnitude of the change and the least detectable change is limited by the noise σ_{\max} . Differences smaller than σ_{\max} are in black while the background is in white. In the first row, sliding DPDs with step $k = 60 \text{ s}$, and in the second row spanning DPDs with step $k = 600 \text{ s}$ are depicted. When the shorter step is used, subtle translocations of cell mass in the area of cell nucleus are clearly visualized. On the other hand, with the longer step, overall changes in cell mass distributions can be shown.

3.2 Osmotic Challenge

As a prime experiment, where the translocation of cell mass should be clearly determined by external conditions, we have chosen the osmotic challenge.

Applicability of digital holographic microscopy for monitoring of osmotic stimulated cell swelling processes was shown already in Ref. 23, where the increasing height during the hypo-osmotic shock was detected. In Ref. 24, short-coherence off-axis holographic phase microscopy was used

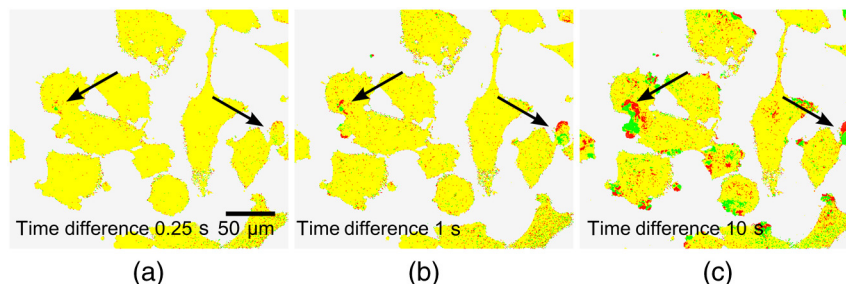


Fig. 3 Incremental DPDs based on a short time interval of 0.25 s. After (a) 0.25 s, (b) 1 s, (c) 10 s, objectives $10\times/0.30$. DPDs of values smaller than σ_{\max} are depicted in yellow color (in contrast to black color used in the following images). Red and green colors represent detectable changes. Arrows highlight spots with intercepted change; we take into account clusters of only few pixels together. This demonstration reveals 1 s to be the time for comparing the speed of action with other cell situations.

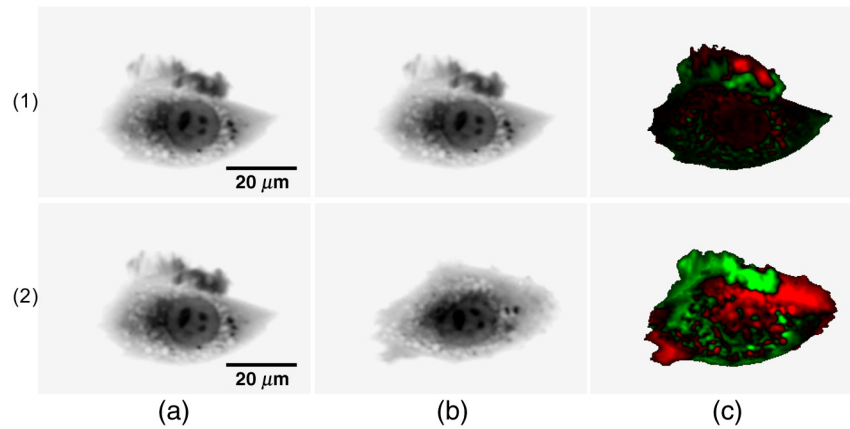


Fig. 4 DPDs of LW13K2 cells. First row: (a) and (b) QPI images of cell, (c) sliding DPDs with a 60 s step. Second row: (a) and (b) QPI images of cell, (c) spanning DPDs with a 600 s step. In an example of sliding DPDs, the emerging pattern of changes are seen and can be used as a trait of cell reaction. In spanning DPDs with longer step, overall changes in mass distribution are shown.

to demonstrate the role of Zn^{2+} ions in suppression of active cell volume regulation. An extensive study of the osmotic challenge in digital holographic microscopy was done in Ref. 25, where the influence of dispersion properties of used media was also considered. They found out that when the dye significantly modifies the extracellular refractive index, the phase signal (cell dry mass) during an osmotic challenge is not only sensitive to variations of cell dry mass spatial distribution, but also to the transmembrane water flux. Also, it was shown that there is practically no phase signal variation during an osmotic challenge when the phase signal is integrated over the entire cell surface area, which indicates conservation of the cell dry mass.

In our study, two types of cell swelling in the lateral and axial directions and their consequences on the measured cell dry mass are shown. We used LW13K2 cells seeded in Ibidi perfusion

chamber (μ -Slide I Luer Family cat. num. 80196) and performed hypo-osmotic shock. The hypo-osmotic shock was induced by change from isotonic medium F10 to medium F10 diluted with water in a ratio of 1:9 and back to isotonic medium F10.

In the first experiment, the cell swelling that occurs mainly in the lateral direction is also noticeable in QPI. However, the translocation in cell mass is not so obvious. In order to get information about these translocations, the time-lapse from the osmotic challenge was evaluated by extended sliding DPDs. The DPDs were calculated with a step $k = 60$ s. In Fig. 5, QPI and the extended sliding DPDs of cells during the swelling and the reverse shrinkage caused by the hypo-osmotic challenge are shown. Swelling and shrinkage are more clearly visible in the extended sliding DPDs, where swelling is identified as red areas located off-center toward the cell boundaries and reverse shrinkage is identified as cyan areas around the cell boundaries.

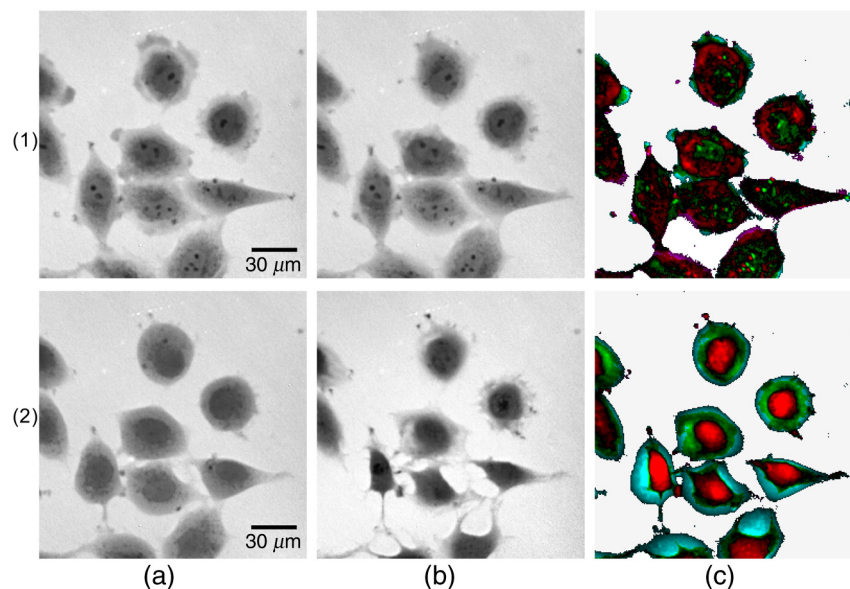


Fig. 5 LW13K2 cells treated with hypotonic medium, objectives $10\times/0.30$. First row: (a) and (b) QPI of cells during the swelling, (c) extended sliding DPDs with a 60-s step; cell swelling is identified as red areas located off-center toward the cell boundaries. Second row: (a) and (b) QPI of cells during the reverse shrinkage, (c) extended sliding DPDs with a 60-s step; cell shrinkage is identified as cyan areas around the cell boundaries.

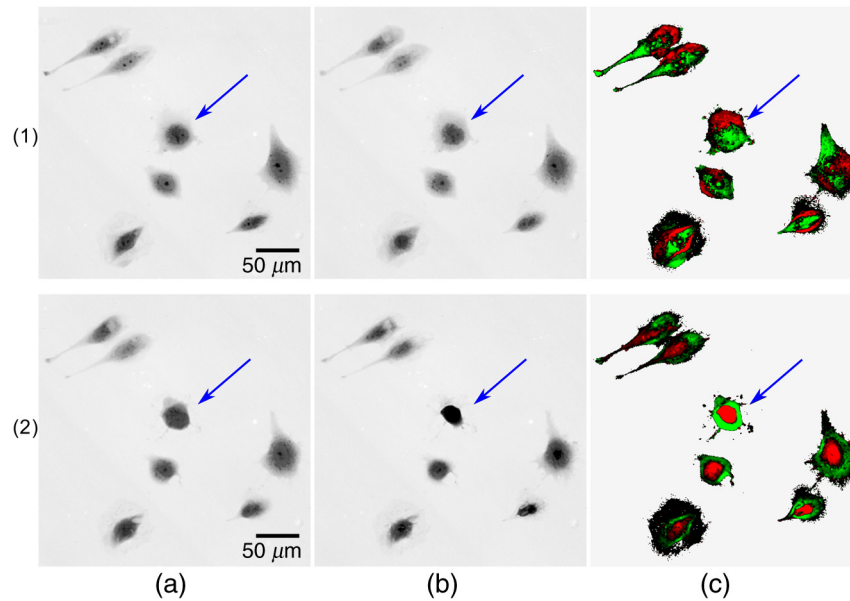


Fig. 6 LW13K2 cells treated with hypotonic medium, objectives $10\times/0.30$. First row: swelling of the cell caused by the change from isotonic medium to hypotonic medium: (a) and (b) QPI from time points 5.5 and 6.5 min, respectively, (c) sliding DPDs with a 60-s step; cell swelling is identified as red areas around the cell boundaries. Second row: shrinkage of the cell, caused by the change from hypotonic to isotonic medium: (a) and (b) QPI from time points 8.5 and 9.5 min, respectively, (c) sliding DPDs with a 60-s step; cell shrinkage is identified as green areas around the cell boundaries. The cell, where swift reaction occurred, is marked.

Figure 6 shows QPI and sliding DPDs from the second experiment. In QPI, changes caused by hypo-osmotic shock are not clearly visible. However, the sliding DPDs with $k = 60$ s distinctly show translocations of cell dry mass. Swelling of the cells caused by the change from isotonic to hypotonic medium is depicted in the first row, where the swelling is clearly identified as red areas around the cell boundaries in the DPDs. Shrinkage of the cells caused by the change from hypotonic to isotonic medium is in the second row and in the DPDs the shrinkage is identified as green areas around the cell boundaries. Sliding DPDs without extension were used because cells did not change their occupied area significantly during the process.

From the DPDs sequence, more dynamic changes in a marked cell are clearly visualized. As a consequence of the change from hypotonic to isotonic medium, the shrinkage of

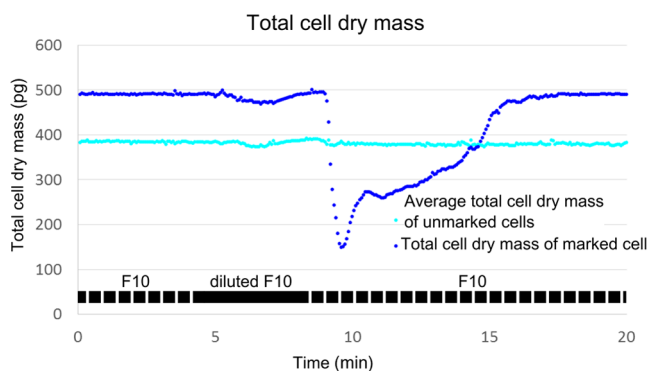


Fig. 7 Cell dry mass during the hypo-osmotic challenge (cells imaged in Fig. 5); light blue: conservation of cell dry mass for cells that remain in depth of focus area; dark blue: cell dry mass decrease for the cell that emerges outside of depth of focus area (marked cell in Fig. 5).

the cell is very rapid and part of the cell emerges outside the depth of the focus area. Because of this, the graph of the cell dry mass remains constant only for the other cells and a decrease in cell dry mass was detected for the marked cell (Fig. 7).

According to biological assumptions during the osmotic challenge, only water perfused through the cell membrane, thus the cell dry mass that corresponds to the phase signal should remain constant.

However, the course of the phase signal also depends on the way of cell swelling and the depth of focus of the used objectives. The influence of the coherence length of the system to the measured phase signal is not considered because the coherence length with the chosen filter (interference filter with central wavelength 650 nm and FWHM 10 nm) is wider than the depth of focus of the chosen objective (Nikon Plan 10/0.3). When the cell swells significantly in the axial direction, a part of it happens to be out of the focus area. The phase signal from this part of the cell cannot be measured properly and a decrease in phase signal is detected. On the other hand, if the swelling occurs mainly in the lateral direction, the whole cell remains in the depth of focus and no change in the phase signal is recorded. Both situations are depicted in a simple scheme in Fig. 8.

4 Conclusion

A DPDs method has been developed in two steps. Originally, the basic DPD method covered the distribution of the dry mass translocation only. Currently, the possibility to develop the extended DPDs has been permitted by the substantial improvement of standard image preprocessing. Thus, changes in the ground plan in terms of new area occupation and vacation could also be taken into account. Both calculations can yield biologically valid information about incremental, sliding, or spanning DPDs. The series of incremental DPDs serve for the speed detection of the minimum cell change. The series

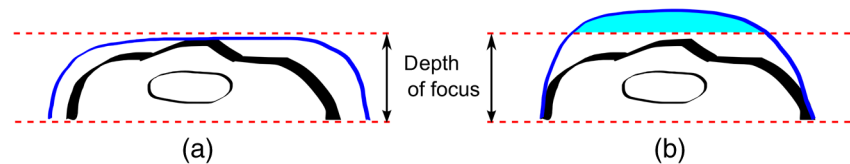


Fig. 8 Possible modes of cell swelling during a hypo-osmotic challenge: (a) if swelling occurs mainly in the lateral direction, the whole cell remains in the depth of focus and the phase signal is measured correctly; (b) if swelling occurs in the axial direction, a part of the cell is outside of the focus area and the phase signal cannot be measured properly. In the figure, the initial state of the cell is black, the state after swelling is the dark blue color, and the area of the cell that cannot be measured properly is the light blue color.

of sliding DPDs detect changes that otherwise may remain unnoticed and can also reveal periodicity in the observed cellular activities. The single image of the spanning DPDs shows overall changes in cell dry mass distribution over a deliberately chosen period of time and can be printed as a 2-D (x, y) snapshot of the three-dimensional (x, y, t) video. Results of the DPDs can be presented either in proportionally color-coded images or numerically in picogram values of transferred mass. The contribution of DPDs in understanding cellular events was shown in an example of cell mitosis and an osmotic challenge experiment. For long time observations, the changes detected by DPDs can be plotted in the graphs and then patterns of live cell behavior can also be statistically analyzed. In the foreseeable future, DPDs graphs could also serve for the automatic acquisition control. QPI exploited by DPDs is a particularly promising new approach to objective characterization of the behavior of cultured cells *in vitro*.

Acknowledgments

This work was supported by CEITEC—Central European Institute of Technology (CZ.1.05/1.1.00/02.0068) from the European Regional Development Fund and Grant Agency of the Czech Republic (15-14612S).

References

- G. Dunn, "Transmitted-light interference microscopy: a technique born before its time," *Proc. R. Microsc. Soc.* **33**, 189–195 (1998).
- B. Rappaz et al., "Measurement of the integral refractive index and dynamic cell morphometry of living cells with digital holographic microscopy," *Opt. Express* **13**, 9361–9373 (2005).
- F. Charriere et al., "Living specimen tomography by digital holographic microscopy: morphometry of testate amoeba," *Opt. Express* **14**, 7005–7013 (2006).
- B. Rappaz et al., "Simultaneous cell morphometry and refractive index measurement with dual-wavelength digital holographic microscopy and dye-enhanced dispersion of perfusion medium," *Opt. Express* **13**, 9361–9373 (2008).
- B. Kemper et al., "Investigation of living pancreas tumor cells by digital holographic microscopy," *J. Biomed. Opt.* **11**, 034005 (2006).
- R. Barer, "Interference microscopy and mass determination," *Nature* **169**, 366–367 (1952).
- G. Dunn et al., "Phase-shifting interference microscopy applied to the analysis of cell behavior," *Symp. Soc. Exp. Biol.* **47**, 91–106 (1993).
- B. Rappaz et al., "Noninvasive characterization of the fission yeast cell cycle by monitoring dry mass with digital holographic microscopy," *J. Biomed. Opt.* **14**, 034049 (2009).
- G. Popescu et al., "Optical imaging of cell mass and growth dynamics," *AJP Cell Physiol.* **295**, C538–C544 (2008).
- P. Girshovitz and N. Shaked, "Generalized cell morphological parameters based on interferometric phase microscopy and their application to cell life cycle characterization," *Biomed. Opt. Express* **3**, 1757–1773 (2012).
- A. Brown and G. Dunn, "Microinterferometry of the movement of dry matter in fibroblasts," *J. Cell Sci.* **92**, 379–389 (1989).
- G. Dunn, "Dynamics of fibroblast spreading," *J. Cell Sci.* **108**, 1239–1249 (1995).
- H. Janeckova, P. Vesely, and R. Chmelik, "Proving tumour cells by acute nutritional/energy deprivation as a survival threat: a task for microscopy," *Anticancer Res.* **29**, 2339–2345 (2009).
- P. Kolman and R. Chmelik, "Coherence-controlled holographic microscope," *Opt. Express* **18**, 21990–22003 (2010).
- T. Slaby et al., "Off-axis setup taking full advantage of incoherent illumination in coherence-controlled holographic microscope," *Opt. Express* **21**, 14747–14762 (2013).
- R. Chmelik et al., "Interferometric system with variable optics for incoherent source of radiation," Czech Patent Application PV 2014-538 (2014).
- T. Zikmund et al., "Sequential processing of quantitative phase images for the study of cell behaviour in real-time digital holographic microscopy," *J. Microsc.* **256**, 117–125 (2014).
- P. Vesely et al., "Spontaneously metastasizing rat sarcomas LW13K2 and RPS: assessment by the immunogenetic test of malignancy, in vitro behaviour and karyology," *Folia Biol.* **35**, 1–12 (1988).
- R. Wayne, "Light and Video Microscopy," 2nd ed., Academic Press (2013).
- T. Kreis, "Digital holographic interference-phase measurement using the Fourier-transform method," *J. Opt. Soc. Am. A* **3**, 847–855 (1986).
- J. Strand, T. Taxt, and A. K. Jain, "Two-dimensional phase unwrapping using a block least-squares method," *IEEE Trans. Image Process.* **8**, 375–386 (1999).
- R. M. Goldstein, H. A. Zebker, and C. L. Werner, "Satellite radar interferometry: two-dimensional phase unwrapping," *Radio Sci.* **23**, 713–720 (1988).
- B. Kemper et al., "Techniques and applications of digital holographic microscopy for life cell imaging," *Proc. SPIE* **6633**, 66330D (2007).
- S. Witte et al., "Short-coherence off-axis holographic phase microscopy of live cell dynamics," *Biomed. Opt. Express* **3**, 2184–2189 (2012).
- D. Boss et al., "Measurement of absolute cell volume, osmotic membrane water permeability, and refractive index of transmembrane water and solute flux by digital holographic microscopy," *J. Biomed. Opt.* **18**, 036007 (2013).

Aneta Krizova is a PhD student at the Brno University of Technology. She received her BS and MS degrees in physical engineering from the Brno University of Technology in 2010 and 2012, respectively. Her current research interests include light microscopy, especially holographic microscopy and its applications.

Jana Collakova is a PhD student at the Brno University of Technology. She received her BS degree in optics from the Palacky University in Olomouc, in 2009 and her MS degree in optics and precise mechanics from the Brno University of Technology in 2011. Her current research interests include digital holographic microscopy in turbid media and living cells imaging.

Zbynek Dostal is a PhD student at the Brno University of Technology. He received his BS degree in mechanical engineering in 2007 and his MS degree in optics and precise mechanics at the Brno University of Technology in 2009. He is a co-author of the CCHM patent for which he received the Werner von Siemens Excellence Award 2013. His

current research interests include holographic microscopy, automation in microscopy, optical, and mechanical design.

Lukas Kvasnica is a PhD student at the Brno University of Technology. He received his MS degree in optics and precise mechanics at the Brno University of Technology in 2008. His current research interests include holographic microscopy and control software development.

Hana Uhlířová is a postdoctoral fellow at the Neurovascular Imaging Laboratory, UCSD. She received her MS degree in optics and precise mechanics and her PhD in applied microscopy from Brno University of Technology in 2006 and 2010, respectively. Her current research is focused on investigation of neurovascular and neurometabolic coupling using two photon imaging and optogenetics and holographic microscopy.

Tomas Zikmund is a junior researcher at the CEITEC, Brno University of Technology. He received his PhD in holographic microscopy at the Brno University of Technology in 2015. Since 2013, he has worked as a head of the x-ray computed micro- and nanotomography laboratory at CEITEC. His main research activity is focused on

development and application of computed tomography (CT) techniques in high-resolution 3D imaging of biological materials and combination CT with other analytical approaches such as laser-induced breakdown spectroscopy.

Pavel Vesely is a senior research scientist at the CEITEC, Brno University of Technology. He received his MD degree at the Charles University in Prague in 1961 and his PhD in experimental biology from the Czechoslovak Academy of Sciences in 1965. He is the author of more than 100 journal papers. His lifelong research interests in cancer cell biology currently include domestication of coherence controlled holographic microscopy in cell biology research.

Radim Chmelik is a professor of applied physics at the Brno University of Technology. He received his MS degree in solid state physics from the Masaryk University in Brno in 1989, and his PhD in physical and materials engineering at the Brno University of Technology in 1997. He is the author of more than 40 journal papers. His current research interests include wave optics, imaging theory, advanced and 3D light microscopy, and holographic microscopy. He is a member of SPIE and OSA.